J. R. Soc. Interface, (2014), 11 (98), 10 p.
DOI: http://dx.doi.org/10.1098/rsif.2014.0484

Uncovering changes in spider orb-web topology owing to aerodynamic effects

Ramón Zaera*, Alejandro Soler and Jaime Teus

Department of Continuum Mechanics and Structural Analysis, University Carlos III of Madrid, 28911 Leganés, Madrid, Spain

* e-mail:ramon.zaera@uc3m.es

Abstract: An orb-weaving spider's likelihood of survival is influenced by its ability to retain prey with minimum damage to its web and at the lowest manufacturing cost. This set of requirements has forced the spider silk to evolve towards extreme strength and ductility to a degree that is rare among materials. Previous studies reveal that the performance of the web upon impact may not be based on the mechanical properties of silk alone, aerodynamic drag could play a role in the dissipation of the prey's energy. Here, we present a thorough analysis of the effect of the aerodynamic drag on wind load and prey impact. The hypo-thesis considered by previous authors for the evaluation of the drag force per unit length of thread has been revisited according to well-established principles of fluid mechanics, highlighting the functional dependence on thread diameter that was formerly ignored. Theoretical analysis and finite-element simulations permitted us to identify air drag as a relevant factor in reducing deterioration of the orb web, and to reveal how the spider can take greater—and not negli-gible—advantage of drag dissipation. The study shows the beneficial air drag effects of building smaller and less dense webs under wind load, and larger and denser webs under prey impact loads. In essence, it points out why the aerodynamics need to be considered as an additional driving force in the evolution of silk threads and orb webs.

Keywords: orb web, aerodynamic drag, wind, impact

1. Introduction

Spider silk is a notable example of an evolved material exhibiting properties, namely outstanding strength and ductility, that make it effective for its use in prey capture [1–5]. While spiders depend upon these properties for survival, evolution has made their silk tougher than almost any other known material [2,6]. Scientists seek to characterize the mechanical behaviour of spider silk under different ambient and load conditions [7–10], to understand the micro-structural reasons for its exceptional performance [4,11,12] and to manufacture threads with similar features [13–15]. Evolution through hundreds of millions of years not only has led to a remarkable material, but also to a consummate struc-tural topology; orb-web spiders braid the threads to build a capture surface that makes the most of the costly silk spun from their glands [5,16].

Many authors have studied the structural features of the orb web under quasistatic [5,6,17–19] or dynamic loading conditions [16,20–22]. A specific feature of the spider webs, which requires a dynamic analysis, is related to the aerodynamic resistance. The drag force owing to the relative motion between the threads and the surrounding air is, by nature, dynamic. Aerodynamic drag implies an increas-ing risk of web destruction by winds [23], but it contributes to the impact resistance of the web. Its role in the dissipation of an insect's kinetic energy has been highlighted by some authors. However, the importance of aerodynamic dis-sipation for the function of orb webs is still unclear. While some studies suggest that it is crucial [23,24], others downplay its importance [25].

Here, we present a thorough analysis of the effect of the aerodynamic drag on wind load and prey impact. The hypothesis considered by previous authors for the evaluation of the drag force per unit length of thread has been revisited according to well-established principles of fluid mechanics. A finite-element model, suitable for treating the nonlinearities characterizing the impact event, was developed and used to identify air drag as a relevant factor in reducing deterioration of the orb

web, and to reveal the interplay between the structural topology of orb webs and the aerodynamic forces enhancing their performance against prey impact.

2. Method and models

Modelling wind load and prey impact on orb webs involves the three characteristic sources of nonlinearities in solid mechanics, namely nonlinear behaviour of materials, finite deformations and contacts. In addition, the web is subjected to a nonlinear aerodynamic force. The short duration of the event and the presence of these nonlinearities make the use of an explicit finite-element code to solve the equilibrium equations recommendable. The explicit solver of the finite-element code Abaqus v. 6.11 [26] was used for this purpose. This section presents the main features of the model as well as the methodology adopted to evaluate degradation of the web.

2.1. Geometry of the orb web

The primary framework of the geometry is idealized as a regular convex polygon tied to a rigid support (boundary conditions of the model) through mooring threads (figure 1*a*). The secondary framework is defined with a set of segments close to the vertices of the polygon. In the capture region, the angular distance between two consecutive radial threads was kept constant. Two spirals were modelled: the hub (logarithmic, small and close to the centre with a high density of spiral threads) and the capture spiral (much larger, Archimedean and located at the periphery of the web). The geometry of the orb web is completely defined by 11 independent parameters: number of sides of the frame N_s and number of radial threads N_r, radius of the polygon R_p, length of the mooring threads L_a, length of the secondary frame threads L_{sf}, initial and final radii of hub spiral (R_{h1} and R_{h2}) and capture spiral (R_{c1} and R_{c2}), length of the logarithmic spiral L_h and separation distance for the Archimedean spiral C_c. Figure 1*a* shows the geometry of an orb web, considered as a *reference case* for the analysis performed in this work (see table 1 for corresponding values, which can be identified by a tilde). This reference web was defined approximating the geometrical characteristics studied elsewhere, and is similar to that considered in the web models presented by other authors [5,12,17,19–22]. The use of a particular geometry prevents the analysis of the features of webs built by specific spiders, given the variability of geometries among species (spider webs exhibit considerable interspecific variability in various aspects), but it has been considered by the authors as a proper methodology to provide a view of the major effects of aerodynamic drag in the mechanical behaviour of orb webs.

2.2. Modelling the silk thread

We may define the stretch λ of the thread as

$$\lambda = \frac{\mathrm{d}x}{\mathrm{d}X}, \tag{2.1}$$

where $\mathrm{d}X$ is the original length of a differential segment and $\mathrm{d}x$ its corresponding deformed length. The Hencky or true strain ε, defined as the natural logarithm of the stretch, was considered. This nonlinear measure of strain is suitable for large deformation phenomena. Multiplicative decomposition

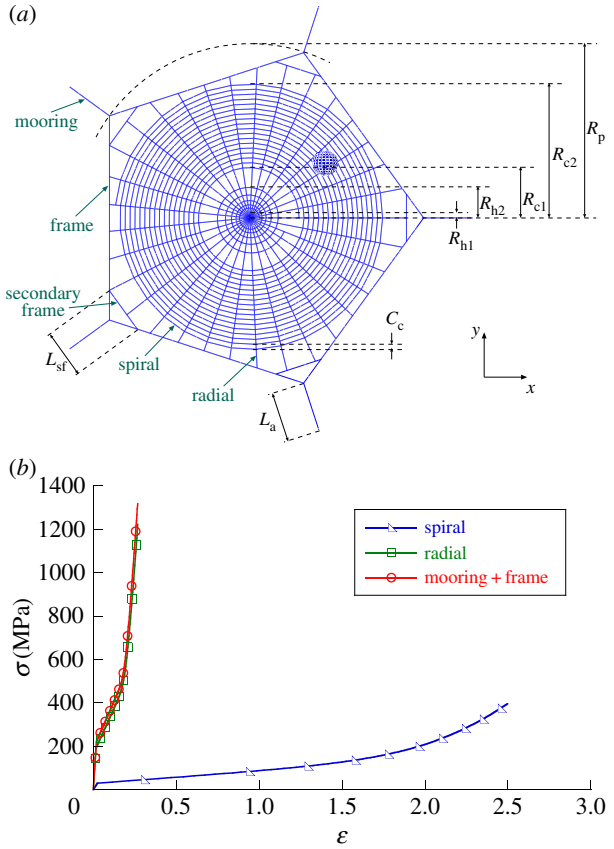

Figure 1. (*a*) Reference orb web with silk thread types, and parameters defining the geometry for a general case. The sphere represents the prey. (*b*) Stress–strain behaviour implemented in the finite-element code for viscid spiral, radial and mooring + frame threads. (Online version in colour.)

Table 1. Values of the parameters defining the geometry reference case (figure 1*a*), approximating the geometrical characteristics studied by Vollrath *et al.* [23].

parameter	variable	value
no. of polygon sides	$\tilde{N}_s$	5
no. of radial threads	$\tilde{N}_r$	33
radius of polygon	$\tilde{R}_p$	141.4 mm
length of mooring threads	$\tilde{L}_a$	40.0 mm
length of secondary frame threads	$\tilde{L}_{sf}$	22.3 mm
initial radius of hub spiral	$\tilde{R}_{h1}$	7.5 mm
final radius of hub spiral	$\tilde{R}_{h2}$	30.0 mm
initial radius of capture spiral	$\tilde{R}_{c1}$	40.0 mm
final radius of capture spiral	$\tilde{R}_{c2}$	110.0 mm
length of logarithmic spiral	$\tilde{L}_h$	0.5 m
separation in Archimedean spiral	$\tilde{C}_c$	4.0 mm

of stretch into recoverable and non-recoverable components automatically leads to the additive decomposition of the strain into its elastic and inelastic parts

$$\varepsilon = \ln(\lambda^e \lambda^p) = \varepsilon^e + \varepsilon^p. \tag{2.2}$$

Deformation of silk essentially takes place under conditions of volume constancy [27]. Then, the actual area of the cross

section of the thread is given in terms of the initial cross section by

$$A = \frac{A_0}{\lambda}. \tag{2.3}$$

We consider the Cauchy or true stress σ, defined as the ratio between the force in the thread F divided by the actual area of the cross section A

$$\sigma = \frac{F}{A}. \tag{2.4}$$

The constitutive behaviour is defined by *Hooke's law*

$$\dot{\sigma} = E\dot{\varepsilon}, \tag{2.5}$$

where E is the Young modulus, the *yield criterion*

$$f(\sigma, \xi) = |\sigma| - \sigma_Y(\xi) = 0, \tag{2.6}$$

where ξ is the hardening parameter and $\sigma_Y(\xi)$ is the *yield stress* given by a phenomenological law (similar to that used by other authors [5] to fit an atomistically derived silk behaviour [4,28])

$$\sigma_Y(\xi) = C + \beta\xi + \alpha_0 \exp(\alpha_1 \xi), \tag{2.7}$$

where C, α_0, α_1 and β are material parameters, the first two being related to the initial yield stress σ_{Y0} through the expression $C = \sigma_{Y0} - \alpha_0$. An *associated plastic flow rule*, the *complementary Kuhn–Tucker conditions*, the *consistency condition* and the *failure strain* $\varepsilon_{\text{fail}}$ complete the constitutive model.

Silk threads show energy dissipation capacity through hysteresis, providing additional damping during unloading. Because the simulations performed in the following study will focus exclusively on the loading process, there is no need to account for the hysteretic behaviour of the material. Similarly, the effect of strain rate has been shown by several authors to enhance the mechanical behaviour of the silk [2,29–32]. However, these effects have not been considered, because the lack of experimental data does not allow variation of initial stiffness, yield flow and failure strain with strain rate to be precisely quantified.

The material parameters are shown in table 2, which have been taken as representative of the nonlinear mechanical behaviour of the three types of silk threads—mooring + frame, radial and viscid spiral—as determined by several authors [2,5,6,20,30,33], without specifying values for particular species. These properties lead to the stress–strain behaviours depicted in figure 1*b*. Table 2 also shows the diameter considered for each type of thread. A value of 1098 kg m^{-3} was assigned for the density of all threads [22]. In order to extend the analyses later presented for a wider range of silk mechanical properties, thus for different silk protein compositions and spinning effects, wide variation in stiffness and failure strain have also been considered. The results will not be presented for brevity, but the trends obtained with the reference silk properties are likewise valid.

Table 2. Thread diameter ϕ and material parameters defining the stress–strain behaviour for mooring + frame, radial and viscid spiral threads (figure 1*b*).

	diameter ϕ (μm)	Young modulus, E (GPa)	initial yield stress, σ_{Y0} (MPa)	β (equation (2.7)) (MPa)	α_0 (equation (2.7)) (Pa)	α_1 (equation (2.7))	strain at failure, $\varepsilon_{\text{fail}}$	plastic work at failure (J m^{-3})
mooring + frame	5.0	12.0	220	2060	0.19	140.2	0.27	6.59×10^7
radial	3.5	12.0	190	1980	3.1	115.5	0.27	6.52×10^7
viscid spiral	2.3	1.2	30	58.9	1.123×10^5	3.53	2.5	2.71×10^8

2.3. Modelling aerodynamic drag

The threads have been idealized as cylinders with circular cross section and constant diameter. The drag coefficient C_D for an infinite cylinder of diameter ϕ varies depending on the Reynolds number Re, which is defined as [34]

$$Re = \frac{|v_n|\phi}{\kappa}, \tag{2.8}$$

where v_n is the normal component of the thread velocity relative to the surrounding air and κ the kinematic viscosity

($\kappa = 16 \times 10^{-6}\,\mathrm{m^2\,s^{-1}}$ for air at 300 K and atmospheric pressure). For the values of silk diameters ($1.9 < \phi < 5\ \mu\mathrm{m}$) and air velocities ($2 < |v_n| < 30.5\,\mathrm{m\,s^{-1}}$) considered in this work, which cover typical silk threads and both prey impact and strong wind conditions, the Reynolds number takes values within $10^{-1} < Re < 10^{1}$. In this range, the relation between drag coefficient C_D and Reynolds number for an infinite circular cylinder is linear, in a log–log graph [34]. Thus, the relation between C_D and Re is approximated by a power law:

$$C_\mathrm{D} = B \cdot Re^{-m} \tag{2.9}$$

with $B = 12.18$ and $m = 0.629$ to fit the experimental results reported by Tritton [35]. The drag force per unit length applied to the silk thread is then given by

$$\boldsymbol{\Psi}_\mathrm{D} = -\frac{1}{2} C_\mathrm{D} \rho_\mathrm{a} \phi |\boldsymbol{v}_n|^2 \boldsymbol{u}_n = -\frac{B}{2} \kappa^m \rho_\mathrm{a} \phi^{1-m} |\boldsymbol{v}_n|^{2-m} \boldsymbol{u}_n, \tag{2.10}$$

where ρ_a is the air density ($\rho_\mathrm{a} = 1.225\,\mathrm{kg\,m^{-3}}$ at 300 K and atmospheric pressure) and $\boldsymbol{u}_n$ the unit vector in the direction of $\boldsymbol{v}_n$. The minus sign means that the force has the opposite direction to that of the normal velocity $\boldsymbol{v}_n$.

Many authors [24,25] considered, as a first approximation, a drag force independent of the diameter in their analysis of aerodynamic effects in spider webs. This hypothesis, resulting from a relationship between the drag coefficient and the Reynolds number with $m = 1$ in equation (2.9), may provide sufficiently accurate results for prey impact conditions ($|\boldsymbol{v}_n| \approx 1\ \mathrm{m\,s^{-1}}$). However, an additional consequence of adopting a value $m = 1$ is the linear dependence on $|\boldsymbol{v}_n|$, which leads to underestimation of the drag force at high velocities, of importance if wind loads are considered. Therefore, a proper description of the drag force applied to a cylinder should consider a relationship between the drag coefficient and the Reynolds number such as that given by equation (2.10) [35–38].

In the case of viscid spiral silk, which is coated with aggregate glue, there is an additional factor to account for because gluey droplets increase the drag force up to value that can be close to 30% higher [24]. The analysis presented herein considers spiral threads with and without droplets in order to show their effect in the overall performance of the web. The presence of droplets has been taken into account increasing by 30% the value given in equation (2.10).

2.4. Internal and external power. Energy absorption and dissipation

Considering stress and strain as homogeneous along a section, the stress power per unit volume may be evaluated by the following expression:

$$\dot{w} = \sigma \frac{\dot{\lambda}}{\lambda} = \sigma \dot{\varepsilon} = \dot{w}^\mathrm{e} + \dot{w}^\mathrm{p}, \tag{2.11}$$

where $\dot{w}^\mathrm{e} = \sigma \dot{\varepsilon}^\mathrm{e}$ is the elastic power and $\dot{w}^\mathrm{p} = \sigma \dot{\varepsilon}^\mathrm{p}$ is the plastic power, both per unit volume. The work dissipated by plastic deformation in the web upon loading is evaluated as

$$\Omega^\mathrm{p} = \int_{V_\mathrm{web}} \int_{t=0}^{t=\hat{t}} \dot{w}^\mathrm{p}\, \mathrm{d}t\, \mathrm{d}V, \tag{2.12}$$

where V_web is the total volume of silk in the web and $\hat{t}$ is the time at which the insect is halted. Plastic work was considered in this paper as a measure that quantifies the degradation of the web produced by a single impact, as described afterwards.

How the kinetic energy of the prey k^e is decreased upon impact is clearly shown through the global power balance considered in the following analysis (web and prey are regarded as a system):

$$\dot{W}^\mathrm{D} = \dot{k}^\mathrm{e} + \dot{K}^\mathrm{e} + \dot{\Omega}^\mathrm{p} + \dot{\Omega}^\mathrm{e}. \tag{2.13}$$

The elastic energy Ω^e owing to recoverable deformation of the silk and the kinetic energy of the web K^e *store* energy, whereas the plastic work Ω^p owing to inelastic deformation of the silk and the work carried out by external forces W^D *dissipate* energy. Because the prey is modelled as rigid, elastic and plastic energies are only measured in the web. To date, no study has quantified the breaking load of the bonds between spiral and radial threads [33]; therefore, additional energy dissipation by the breaking of thread junctions is not accounted for in the power balance. The external work rate is calculated through the integral of power developed by the drag force over the whole length of silk threads L_web

$$\dot{W}^\mathrm{D} = \int_{L_\mathrm{web}} \boldsymbol{\Psi}_\mathrm{D}\, \boldsymbol{v}_n\, \mathrm{d}L. \tag{2.14}$$

Because $\boldsymbol{\Psi}_\mathrm{D}$ and $\boldsymbol{v}_n$ have opposite directions, the external work will be negative, which is consistent with the power balance provided by equation (2.13).

2.5. Finite-element model

The silk threads were modelled with two-node linear displacement truss elements. Cable-like behaviour of the spider silk thread was forced by setting at least two elements in each segment of the web, which introduces at least an intermediate hinge along each segment to capture the low bending stiffness of such a slender thread. This way, just a slight compressive force induced in the thread leads to misalignment of the elements, which immediately reduces its value. Peak compressive forces in the web were found during the analysis of the simulations to be three orders of magnitude lower than yield forces. The small characteristic size of the element along the mesh, defined by the smallest spiral segment between two radii, served also to softly match the spherical geometry of the prey upon contact, and to satisfy the mesh convergence analysis. Additionally, simulations of a transversally impacted thread were performed to verify the propagation of both longitudinal and transverse waves in the linear elastic range, and the results were satisfactorily validated against the corresponding theoretical solution [39].

As stated in [17,20,21,40], orb-web spiders control pretensile forces in threads during web construction to gain structural stability. In this work, the reference configuration of the web was assumed to be unstretched and, consequently, unloaded. However, complementary simulations were performed considering pre-stress in the silk threads. The results will not be presented for brevity, but the trends obtained with the unstressed web can also be extended to the pre-stressed case (see electronic supplementary material).

The set of nonlinear constitutive equations are integrated through an implicit stress update algorithm implemented in a user subroutine. Regarding the aerodynamic drag force, equation (2.10) was also implemented in the finite-element

code through a user subroutine. The adhesive effect produced by viscid capture threads was likewise incorporated in the model.

The prey was modelled as a rigid surface in the finite-element model, given the lack of representative stiffness values available in the literature. Various sources were consulted to define the geometrical characteristics of the prey [29,41,42]. Owing to the variability found among species, a representative shape was used: a sphere with a diameter of 20 mm weighing 3×10^{-5} kg, the size based on that of honeybees or grasshoppers. A reference value of the impact velocity $V_0 = 2\ \mathrm{m\ s^{-1}}$ was assumed, and at normal incidence to the web plane $\{x,y\}$. The same relative position of the impact point was used for all the different analyses; in the bisectrix of a sector of the polygon and halfway along the radial segment of the capture spiral (figure 1*a*), because prey impacts are eccentric in most cases. As commonly assumed in impulsive events, gravitational forces have been neglected. Regarding wind conditions, the loading process was simulated by progressively increasing air velocity in the direction normal to the reference web plane.

It is worth pointing out that the vibrational behaviour of the web does not play a role during the loading stage. Certainly, high-frequency oscillations are present during this stage, but the numerical simulations confirmed that their amplitude is negligible. Once the prey has stretched the web up to its maximum deflection and starts to recoil, the global vibration of the web contributes to dissipate the stored elastic energy. However, the analysis performed in our work focuses on the degradation induced by prey impact which, according to the results of the simulations, develops just during the first loading phase. Therefore, vibrational dissipation of energy (by aerodynamic drag or hysteresis in silk threads) does not contribute to diminish degradation in the web.

Regarding the influence of permanent spiral threads, retained by *Nephila* spiders in their webs, their structural role has been recently studied by Hesselberg & Vollrath [40]. Considering exclusively aerodynamic aspects, it is reasonable to think that the presence of non-sticky spiral silk would not result in a higher drag because it is placed within gaps of the sticky spiral, replacing it rather than adding one.

2.6. Plastic work as a measure of the degradation in the web

Energy absorbers in crashworthiness or ballistic applications are commonly designed with materials that are capable of keeping a high value of stress upon deformation and able to show a large value of strain at failure [43,44]. In this way, the material enables higher values of energy to be dissipated through inelastic strain. Moreover, the structural typology is designed to deliberately generate substantial deformation and damage for a purpose of absorbing as much kinetic energy as possible. Thus, an impact protection showing intense and extended inelastic strains upon deformation is considered as an efficient system. In other words, they are designed as *single-use* elements, such as the bumpers of a car or the panels of an armour, which are commonly changed after the impact event as soon as damage is visible. However, an orb web has no additional armour to preserve its primary prey-capture function. That is, it has to protect itself from the impact. Therefore, one of the most important structural features of a spider web should be its multi-hit capability: the ability to withstand a number of prey impacts before failure. This will save the nutritional resources required to rebuild a web in the event of partial failure, or to build a new one in the event of complete failure. Regarding its impact response, a spider web can be considered as a *reusable* system.

A low harmful impact would be that producing only elastic strains; in such a case, the mechanical properties of the web will remain the same. But, higher impact velocities may produce inelastic strains in some threads, leading to a certain level of *degradation* in the web: it will remain slack (having greater accelerations), damage processes start to develop at the microstructural level [4,28] and the amount of energy that can be dissipated by deformation before failure decreases. Thus, each impact involving inelastic strains may be considered as a cumulative damage event in a process that eventually leads to failure.

A simple yet reliable method to account for cumulative degradation in structures subjected to the effect of dynamic cyclic loading is through plastic energy concepts. Similar approaches are commonly used to quantify the severity of dynamic cycling loading for practical seismic design [45]. According to this methodology, the plastic work dissipated in the web Ω^{p} can be used as a direct measure of the severity of the loading process. The proposed approach is macroscopic in the sense that Ω^{p} is a global measure, and that the distribution of plastic work among the different threads is not represented here. However, it permits a rapid evaluation of the degradation in the web after one loading event and a quantitative comparison between the efficiency of different web architectures.

3. Changes in the orb-web geometry modify the drag force

A closed-form expression to approximate the aerodynamic force acting on the capture area of the web will be derived. Mooring and frame threads are excluded from this expression, because their lengths (therefore the associated drag force) are commonly much less than those of radial and spiral threads.

We may consider a baseline geometry of the capture zone with external radius $\tilde{R}$, angular distance between radial threads $\tilde{\delta}_{\mathrm{r}}$ and distance between spiral threads $\tilde{\delta}_{\mathrm{s}}$. The reference silk diameters are $\tilde{\phi}_{\mathrm{r}}$ for radial threads and $\tilde{\phi}_{\mathrm{s}}$ for spiral threads. For the sake of simplicity, the Archimedean spiral extends from the centre to the outer limit of the capture area ($0 \leq r \leq \tilde{R}$), thus the hub is obviated. Starting from this reference web, variations in size are now introduced through a scale factor α_H affecting both $\tilde{R}$ and $\tilde{\delta}_{\mathrm{s}}$; this factor permits one to obtain a thread pattern homothetic to the baseline geometry. Let us consider additional changes in the geometry through two new scale factors, the first one α_δ scaling separation between threads of the same family (both radial and spiral) and the second one α_ϕ scaling simultaneously the diameter of both types of thread (figure 2).

The following equations are obtained through a continualization process in which the web composed of discrete threads is changed by a continuum. This permits one to derive, taking advantage of the differential and integral calculus, useful expressions for the analysis of air drag effects.

Figure 2 shows a part of this ideal capture zone. Considering a sector of this web centred in the intersection between

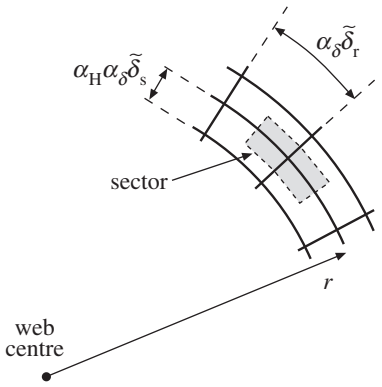

Figure 2. Sector of the capture area for the estimation of the drag force.

two threads at a position r, the lengths of radial and spiral silk on it are given by

$$L_r = \alpha_H \alpha_\delta \tilde{\delta}_s \tag{3.1}$$

and

$$L_s = r\alpha_\delta \tilde{\delta}_r \tag{3.2}$$

and the sector area by

$$A = \alpha_H \alpha_\delta^2 \tilde{\delta}_r \tilde{\delta}_s r. \tag{3.3}$$

Thus, the areal density of silk length for each type of thread is

$$\eta_r = \frac{L_r}{A} = \frac{1}{\alpha_\delta \tilde{\delta}_r r} \tag{3.4}$$

and

$$\eta_s = \frac{L_s}{A} = \frac{1}{\alpha_H \alpha_\delta \tilde{\delta}_s}. \tag{3.5}$$

Equations (2.10), (3.4) and (3.5) permit one to estimate the drag force acting on radial and spiral threads through the following expressions:

$$F_r = 2\pi \int_0^{\alpha_H \tilde{R}} \eta_r \Psi_D r \, dr \tag{3.6}$$

and

$$F_s = 2\pi \int_0^{\alpha_H \tilde{R}} \eta_s \Psi_D r \, dr. \tag{3.7}$$

3.1. Drag upon wind load

Taking $v_n = v_{wind}$ in equation (2.10), the drag force acting on the capture area is

$$F_{wind} = F_{wind,r} + F_{wind,s} = \Lambda_\alpha \tilde{F}_{wind}, \tag{3.8}$$

where $\tilde{F}_{wind}$ is the drag force corresponding to the baseline web

$$\tilde{F}_{wind} = \pi B \kappa^m \rho_a \tilde{R} \left(\frac{\tilde{\phi}_r^{1-m}}{\tilde{\delta}_r} + \frac{\tilde{R}\,\tilde{\phi}_s^{1-m}}{2\tilde{\delta}_s} \right) v_{wind}^{2-m} \tag{3.9}$$

and Λ_α is a *web-drag coefficient* depending on the three scale factors

$$\Lambda_\alpha = \frac{\alpha_H \alpha_\phi^{1-m}}{\alpha_\delta}. \tag{3.10}$$

3.2. Drag upon impact load

Considering for the sake of simplicity a centred impact and boundary conditions acting at the outer periphery of the capture zone, we may assume the following linear velocity profile in the web:

$$v_n = v_{prey} \left(1 - \frac{r}{\alpha_H \tilde{R}} \right), \tag{3.11}$$

where v_{prey} is the velocity at the centre of the web, coincident with that of the prey. The drag force acting on the capture area is then

$$F_{prey} = F_{prey,r} + F_{prey,s} = \Lambda_\alpha \tilde{F}_{prey}, \tag{3.12}$$

where $\tilde{F}_{prey}$ is the drag force corresponding to the baseline web

$$\tilde{F}_{prey} = \pi B \kappa^m \rho_a \tilde{R} \left(\frac{\tilde{\phi}_r^{1-m}}{\tilde{\delta}_r (3-m)} + \frac{\tilde{R}\,\tilde{\phi}_s^{1-m}}{\tilde{\delta}_s (4-m)(3-m)} \right) v_{prey}^{2-m} \tag{3.13}$$

and the web-drag coefficient Λ_α has the same expression obtained for wind load (equation (3.10)).

3.3. Influence of geometrical scale factors on web drag

Spiders do not have control over the parameters κ, ρ_a, B and m in equations (3.9) and (3.13). On the contrary, the spider may include structural changes in the orb-web through the scale factors α_H and α_δ. The coefficient Λ_α, which groups the scaling factors, permits one to understand how changes in the geometry of the web may modify aerodynamic forces under wind or impact loads: an increase in web size, as well as a decrease in the distances between threads of the same family (radial or spiral), raises drag.

Among the different abovementioned aspects driving the web geometry, manufacturing costs play a key role. As stated by several authors [46–48], energy investment in webs is properly characterized through the total volume of silk, most of which is linked to the capture area. By following the previous approach, this volume can be estimated as

$$\begin{aligned} V &= 2\pi \int_0^{\alpha_H \tilde{R}} \frac{\pi \alpha_\phi^2}{4} (\eta_r \tilde{\phi}_r^2 + \eta_s \tilde{\phi}_s^2) r \, dr \\ &= \frac{\alpha_H \alpha_\phi^2}{\alpha_\delta} \frac{\pi^2 \tilde{R}}{2} \left(\frac{\tilde{\phi}_r^2}{\tilde{\delta}_r} + \frac{\tilde{R}\,\tilde{\phi}_s^2}{2\tilde{\delta}_s} \right). \end{aligned} \tag{3.14}$$

Thus, variations in the web geometry fulfilling the following condition:

$$2\alpha_H \alpha_\delta \alpha_\phi d\alpha_\phi - \alpha_H \alpha_\phi^2 d\alpha_\delta + \alpha_\delta \alpha_\phi^2 d\alpha_H = 0, \tag{3.15}$$

keep constant the silk volume invested in the capture zone. If the overall size of the capture zone remains unchanged (α_H constant), thus keeping constant the area available to intercept prey, equation (3.15) can be integrated leading to the following relation between diameter and thread-spacing factors:

$$\alpha_\phi^2 = \alpha_\delta \tag{3.16}$$

and the web-drag coefficient becomes

$$\Lambda_\alpha = \frac{\alpha_H}{\alpha_\delta^{(1+m)/2}}. \tag{3.17}$$

The distance between threads of the same family therefore emerges as a key parameter that may contribute to decrease drag force under wind load (higher α_δ) or to increase drag dissipation under impact load (lower α_δ). Certainly, at equal raw

material costs, this requires a higher or a lower thread diameter α_ϕ, respectively.

Similarly, we may determine the web-drag coefficient corresponding to a variation of the capture area at constant silk volume. Keeping constant α_δ and permitting variations of α_H and α_ϕ, integration of equation (3.15) leads to the relation

$$\alpha_\phi = \sqrt{\frac{1}{\alpha_H}}, \tag{3.18}$$

and the web-drag coefficient becomes

$$\Lambda_\alpha = \frac{\alpha_H^{(1+m)/2}}{\alpha_\delta}. \tag{3.19}$$

Thus, spiders may increase or decrease the drag force by increasing or decreasing the size of the web (α_H), respectively. Both equations (3.17) and (3.19) reflect the effect of increasing the thread length at the expense of reducing the thread diameter, leading to a higher aerodynamic drag—at equal silk volume.

Coupled aerodynamics–structural analyses will be performed in the following sections in order to uncover how the spider may enhance the performance of the orb-web (under wind load or prey impact) through the introduction of suitable modifications in the geometry, taking advantage of the aerodynamic effects. All these analyses will be performed under the hypothesis of *silk volume constancy*. There is a strong tendency in the world of biology to make the maximum use of finite resources; saving operational energy allows the organism to spend more energy to reproduce. Adding a constraint of constant silk volume to this study permits a valuable insight into the way energetic resources are used by spiders in a more efficient way. The results obtained with this constraint permit one to show how and why the spider can adapt web design to service conditions, reaching higher structural efficiency at constant silk expenditure. Additionally, keeping constant the amount of silk allows one to preserve the structural features of the web roughly unchanged, as will be shown subsequently, and therefore to focus specifically on the aerodynamic effects.

Section 4 presents the results corresponding to wind and impact load, which will be discussed in the last section of the article.

4. Aerodynamic drag upon wind or impact load

On the basis of the reference web geometry, additional geometries were generated by scaling either the distances between threads of the same family (spiral and radial) by the factor α_δ, or the web size by the factor α_H. A unit value of α_δ and α_H corresponds to the mesh geometry shown in table 2.

Because the current analysis focuses specifically on the aerodynamic effects, mooring and frame threads have been excluded from scaling in the diameter, because this would strongly modify the structural behaviour of the web.

4.1. Wind load

Let us define the *critical wind velocity* as that leading to the collapse of the web, characterized by the failure of a mooring thread (breakage of one of these threads strongly compromises the primary prey-capture function for the geometry considered in this work). This critical velocity was calculated with the finite-element code, and its dependence on distances between threads of the same family α_δ and web size α_H is presented in figure 3*a*,*b*, respectively. Likewise, each figure shows the influence of α_δ and α_H on the drag force.

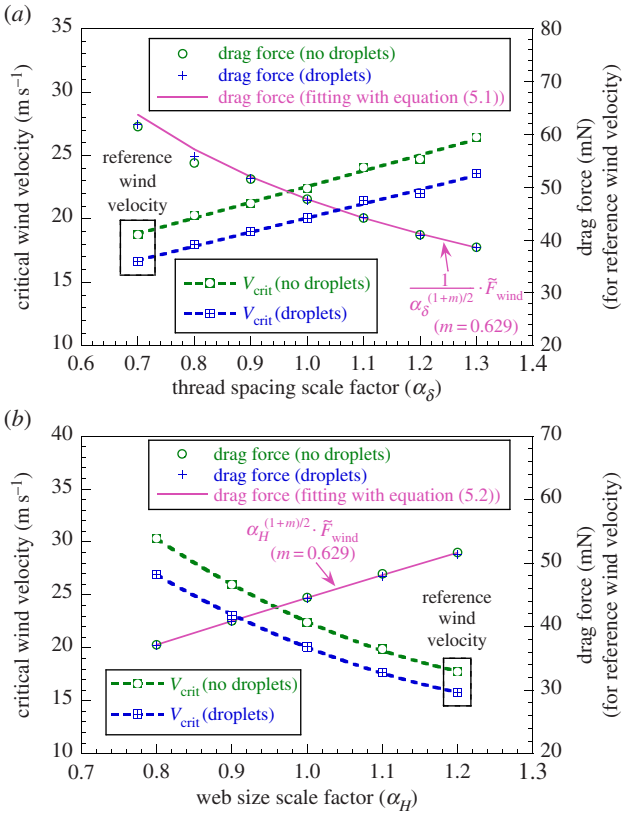

Figure 3. (*a*) Influence of the distances between threads of the same family (radial and spiral) on critical wind velocity (finite-element results), and on drag force at $v_{wind} = 18.7$ m s^{-1} (finite-element results and analytical approach). (*b*) Influence of web size on critical wind velocity (finite-element results), and on drag force at $v_{wind} = 17.7$ m s^{-1} (finite-element results and analytical approach). Analysis at constant silk volume. (Online version in colour.)

It is worth pointing out that the thread diameters resulting from the variation in α_δ and α_H are reasonable, $0.84 \leq \alpha_\phi \leq 1.14$ according to equations (3.16) and (3.18), keeping in mind that some authors found that thread diameters within webs of individual spiders can vary by as much as 600% [49].

4.2. Impact load

Impacts of the reference prey onto the webs defined by variations in α_δ and α_H were simulated with the finite-element code, and the corresponding results are shown in figure 4*a*,*b*. Now, the scale ratio α_H ranges from 0.3 to 1.2, which covers the range of orb-web sizes woven by small and large spiders. The thread diameters resulting from the variation in α_δ and α_H are $0.84 \leq \alpha_\phi \leq 1.82$. Plastic work, without and with drag, and aerodynamic work are determined, the former being included in order to keep track of degradation of the web.

5. Discussion

According to figure 3*a*, the web is more efficient under wind loads when the spider spins a less dense capture area: it can withstand stronger winds when using larger distance between radial and between spiral threads. The improvement in the structural behaviour of the web is due to the reduction of the drag force, as seen in figure 3*a*. It becomes clear that gluey

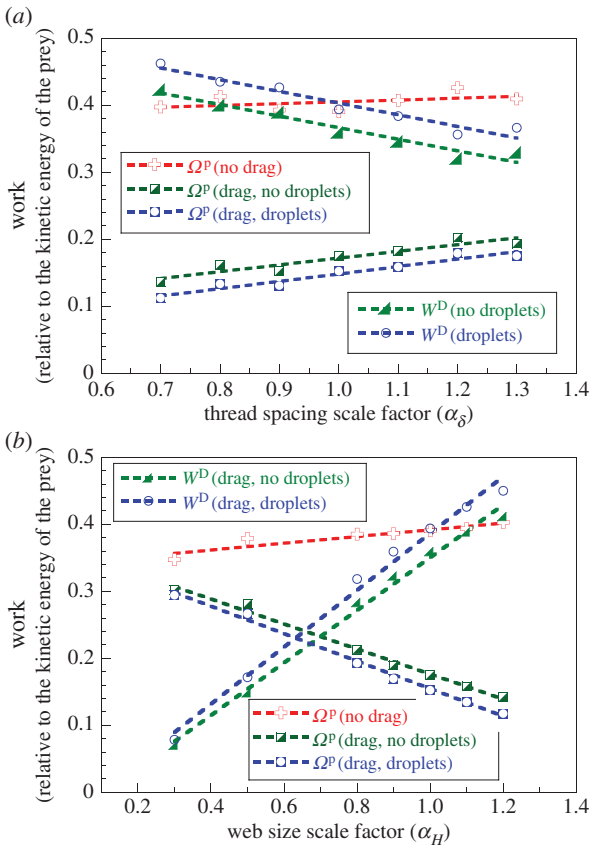

Figure 4. (*a*) Influence of the distances between threads of the same family (radial and spiral) on plastic work and aerodynamic work. (*b*) Influence of web size on plastic work and aerodynamic work. Analysis at constant silk volume. (Online version in colour.)

droplets lead to lower values of the critical wind velocity. Moreover, the influence of α_δ in the drag force is properly captured by the web-drag coefficient defined in equation (3.8)

$$F_{\text{wind}} = \frac{\tilde{F}_{\text{wind}}}{\alpha_\delta^{(1+m)/2}}, \tag{5.1}$$

where the condition given by equation (3.17) and $\alpha_H = 1$ (constant capture area, and equal to that of the reference web) were considered. In figure 3*a*, the reference drag force $\tilde{F}_{\text{wind}}$ corresponding to $\alpha_\delta = 1$ has been obtained from the finite-element results.

Likewise, figure 3*b* shows how the web is more efficient under wind loads when the size of the capture area is smaller (at equal silk volume): according to the simulation results, it can withstand stronger winds when spinning smaller webs, with or without droplets. The improvement in the structural behaviour of the web is due to the reduction of the drag force, as seen in figure 3*b*. The variation of the drag force is also captured by the web-drag coefficient defined in equation (3.8)

$$F_{\text{wind}} = \alpha_H^{(1+m)/2}\, \tilde{F}_{\text{wind}}, \tag{5.2}$$

where the condition given by equation (3.19) and $\alpha_\delta = 1$ were considered. In figure 3*b*, the reference drag force $\tilde{F}_{\text{wind}}$ corresponding to $\alpha_H = 1$ has been obtained from the finite-element results.

The previous analysis is consistent with the results of Liao *et al.* [50], who examined how aerodynamic forces affected the structural properties of orb webs built by *Cyclosa* spider species inhabiting areas with different levels of wind disturbances. As concluded by those authors, 'To cope with strong winds, orb spiders inhabiting seashore area build smaller and less dense webs with thicker and stronger silk threads'. Similar results were obtained by other authors [23,51,52], who showed that spiders reduce radii number, spiral length and capture area when they detect a windy environment. Looked at in another way, in the absence of strong winds, when prey impact becomes the most relevant load, the spiders may take advantage of spinning larger and denser webs. Next, we will clarify the reasons behind such behaviour.

According to figure 4*a*, the benefit of using different distances between threads of the same family (radial and spiral) under impact loading without the effect of drag forces is not clear: the plastic work experiences just a slight decrease for a large reduction in α_δ, which can be assumed to be owing to more uniform distribution of the contact force among the various elements of the structure (smaller distance between threads). Obviously, this is a consequence of assuming the constraint of constant silk volume, which preserves the amount of structural material present in the web. However, we find a clear advantage to using closer spacing when drag forces are considered: the plastic work undergoes a strong decrease. This effect is clearly owing to an increase in the work performed by the aerodynamic forces, as shown in figure 4*a*. It becomes manifest that gluey droplets lead to lower values of the plastic work. Likewise, the benefits of spinning large webs under impact loading become evident when considering the effect of the drag (figure 4*b*). Both longer threads in the capture area and higher out-of-plane compliance, which permits higher velocities and displacements of the web, lead to greater dissipation of energy owing to drag. By the same rule, small webs do not benefit from the aerodynamic force; as figure 4*b* shows, the difference between the plastic work without and with drag is barely notable for the smallest web considered in the analysis. Thus, the spiders that gain the most from aerodynamic drag are those building larger webs.

According to the present analysis, spiders find a clear advantage to modifying the web topology depending on the loading conditions. Certainly, there are other factors conditioning the geometry of the web. For instance, a smaller thread spacing permits catching smaller prey, and a larger web increases the capture area and the probability of prey interception [53]; on the other hand, larger silk length implies higher building and behavioural costs. Likewise, the pressure to capture large prey in order to boost the energetic gain and ensure reproductive success dictates additional requirements for web size and of the distances between threads [54,55]. In any case, in the strong evolutionary tension between topological changes in webs that enhance prey interception and retention and those that reduce energetic costs, the interplay between geometry and drag should be considered as an additional driving factor in the evolution of web architecture and silk biomechanics. The benefits of changing the web topology for either increasing or decreasing aerodynamic drag are too high to be disregarded in the evolutionary process.

Acknowledgements. We express our sincere gratitude to Alejandro Sevilla (Univ. Carlos III), to Sidney Chocrón (Southwest Research Institute, TX), to Daniel Rittel (Technion) and to José Fernández-Sáez (Univ. Carlos III), for helpful discussions.

Data accessibility. Supplementary information on the influence of web pre-stress can be found at Dryad: doi:10.5061/dryad.24k4r.

References

1. Vollrath F. 1992 Spider webs and silks. *Sci. Am.* **266**, 70–76. (doi:10.1038/scientificamerican0392-70)
2. Gosline J, Guerette P, Ortlepp C, Savage K. 1999 The mechanical design of spider silks: from fibroin sequence to mechanical function. *J. Exp. Biol.* **202**, 3295–3303.
3. Vollrath F. 2003 Web masters. *Nature* **426**, 121–122. (doi:10.1038/426121a)
4. Keten S, Buehler M. 2010 Nanostructure and molecular mechanics of spider dragline silk protein assemblies. *J. R. Soc. Interface* **7**, 1709–1721. (doi:10.1098/rsif.2010.0149)
5. Cranford S, Tarakanova A, Pugno N, Buehler M. 2012 Nonlinear material behaviour of spider silk yields robust webs. *Nature* **482**, 72–76. (doi:10. 1038/nature10739)
6. Boutry C, Blackledge T. 2009 Biomechanical variation of silk links spinning plasticity to spider web function. *Zoology* **112**, 451–460. (doi:10. 1016/j.zool.2009.03.003)
7. Osaki S. 1996 Spider silk as mechanical lifeline. *Nature* **384**, 419. (doi:10.1038/384419a0)
8. Guinea G, Elices M, P´erez-Rigueiro J, Plaza G. 2005 Stretching of supercontracted fibers: a link between spinning and the variability of spider silk. *J. Exp. Biol.* **208**, 25–30. (doi:10.1242/jeb.01344)
9. Liu Y, Shao Z, Vollrath F. 2005 Relationships between supercontraction and mechanical properties of spider silk. *Nat. Mater.* **4**, 901–905.(doi:10.1038/nmat1534)
10. Elices M, Plaza G, Arnedo M, P´erez-Rigueiro J, Torres F, Guinea G. 2009 The mechanical behaviour of silk during the evolution of orb-web spinning spiders. *Biomacromolecules* **10**, 1904–1910. (doi:10.1021/bm900312c)
11. Ayoub N, Garb J, Tinghitella R, Collin M, Hayashi C. 2007 Blueprint for a high-performance biomaterial: full-length spider dragline silk genes. *PLoS ONE* **2**, e514. (doi:10.1371/journal.pone.0000514)
12. Askarieh G *et al*. 2010 Self-assembly of spider silk proteins is controlled by a pH-sensitive relay. *Nature* **465**, 236–238. (doi:10.1038/nature08962)
13. Tarakanova A, Buehler M. 2012 A materiomics approach to spider silk: protein molecules to webs. *JOM* **64**, 214–225. (doi:10.1007/s11837-012-0250-3)
14. Xia X, Qian Z, Kib C, Park Y, Kaplanc D, Lee S. 2010 Native-sized recombinant spider silk protein produced in metabolically engineered *Escherichia coli* results in a strong fiber. *Proc. Natl Acad. Sci. USA* **107**, 14 059–14 063. (doi:10.1073/pnas.1003366107)
15. Teule F, Miao Y-G, Sohn BH, Kim Y, Hull J, Fraser M, Lewis R, Jarvis DL. 2012 Silkworms transformed with chimeric silkworm/spider silk genes spin composite silk fibers with improved mechanical properties. *Proc. Natl Acad. Sci. USA* **109**, 923–928.(doi:10.1073/pnas.1109420109)
16. Craig C. 1987 The ecological and evolutionary interdependence between architecture and web silk spun by orb web weaving spiders. *Biol. J. Linn. Soc.* **30**, 135–162. (doi:10.1111/j.1095-8312.1987. tb00294.x)
17. Lin L, Sobek W. 1998 Structural hierarchy in spider webs and spiderweb-type systems. *Struct. Eng.* **76**, 59–64.
18. Aoyanagi Y, Okumura K. 2010 Simple model for the mechanics of spider webs. *Phys. Rev. Lett.* **104**, 038102. (doi:10.1103/PhysRevLett.104.038102)
19. Tarakanova A, Buehler M. 2012 The role of capture spiral silk properties in the diversification of orb webs. *J. R. Soc. Interface* **9**, 3240–3248. (doi:10. 1098/rsif.2012.0473)
20. Alam M, Jenkins C. 2005 Damage tolerance in naturally compliant structures. *Int. J. Damage Mech.* **14**, 365–384. (doi:10.1177/1056789505054313)
21. Alam M, Wahab M, Jenkins C. 2007 Mechanics in naturally compliant structures. *Mech. Mater.* **39**, 145–160. (doi:10.1016/j.mechmat.2006.04.005)
22. Ko F, Jovicic J. 2004 Modeling of mechanical properties and structural design of spider web. *Biomacromolecules* **5**, 780–785. (doi:10.1021/bm0345099)
23. Vollrath F, Downes M, Krackow S. 1997 Design variability in web geometry of an orb-weaving spider. *Physiol. Behav.* **62**, 735–743. (doi:10.1016/S0031-9384(97)00186-8)
24. Lin L, Edmonds D, Vollrath F. 1995 Structural engineering of an orb-spider web. *Nature* **373**, 146–148. (doi:10.1038/373146a0)
25. Sensenig A, Lorentz K, Kelly S, Blackledge T. 2012 Spider orb webs rely on the radial threads to absorb prey kinetic energy. *J. R. Soc. Interface* **9**, 1880–1891. (doi:10.1098/rsif.2011.0851)
26. Simulia. 2013 *ABAQUS/explicit user's manual. v. 6.11.2 ed*. Providence, MD: Dassault Systemes.
27. Guinea G, Pe´rez-Rigueiro J, Plaza G, Elices M. 2006 Volume constancy during stretching of spider silk. *Biomacromolecules* **7**, 2173–2177. (doi:10.1021/bm060138v)
28. Keten S, Xu Z, Ihle B, Buehler M. 2010 Nanoconfinement controls stiffness, strength and mechanical toughness of β-sheet crystals in silk. *Nat. Mater.* **9**, 359–367. (doi:10.1038/nmat2704)
29. Denny M. 1976 The physical properties of spider's silk and their role in the design of orb-webs. *Exp. Biol.* **65**, 483–506.
30. Cunniff P, Fossey A, Auerbach M, Song J, Kaplan D, Adams W, Eby RK, Mahoney D, Vezie DL. 1994 Mechanical and thermal properties of dragline spider silk from the spider *Nephila clavipes*. *Polym. Adv. Technol.* **5**, 401–410. (doi:10.1002/pat.1994. 220050801)
31. Drodge D, Mortimer B, Holland C, Siviour C. 2012 Ballistic impact to access the high-rate behaviour of individual silk fibres. *J. Mech. Phys. Solids* **60**, 1710–1721. (doi:10.1016/j.jmps. 2012.06.007)
32. Hudspeth M, Nie X, Chen W, Lewis R. 2012 Effect of loading rate on mechanical properties and fracture morphology of spider silk. *Biomacromolecules* **13**, 2240–2246. (doi:10.1021/bm3003732)
33. Blackledge T, Kuntner M, Agnarsson I. 2011 The form and function of spider orb webs: evolution from silk to ecosystems. *Adv. Insect Physiol.* **41**, 175–262. (doi:10. 1016/B978-0-12-415919-8.00004-5)
34. Tritton D. 1988 *Physical fluid dynamics*. Oxford, UK: Oxford University Press.
35. Tritton D. 1959 Experiments on the flow past a circular cylinder at low Reynolds numbers. *J. Fluid Mech.* **6**, 547–567. (doi:10.1017/S0022112059000829)
36. Oseen C. 1910 Uber die stokessche formel und u¨ber eine vervandte aufgabe in der hydrodynamik. *Arkiv. Matematik, Astronomi och Fysik* **6**, 175.
37. Lamb H. 1932 *Hydrodynamics*. Cambridge, UK: Cambridge University Press.

38. Jayaweera K, Mason B. 1965 The behaviour of freely falling cylinders and cones in a viscous fluid. *J. Fluid Mech.* **29**, 709–720. (doi:10.1017/S002211206 500109X)
39. Smith J, McCracken F, Schiefer H. 1958 Stressstrain relationships in yarns subjected to rapid impact loading. Part V: wave propagation in long textile yarns impacted transverselly. *Textile Res. J.* **28**, 288–302. (doi:10.1177/004051755802800402)
40. Hesselberg T, Vollrath F. 2012 The mechanical properties of the non-sticky spiral in *Nephila* orb web (Araneae, Nephilidae). *Exp. Biol.* **215**, 3362–3369. (doi:10.1242/jeb.068890)
41. Prokop P. 2008 Prey type does not determine web design in two orb-weaving spiders. *Zool. Stud.* **45**, 124–131.
42. Blackledge T, Zevenbergen J. 2007 Condition-dependent spider web architecture in the western black widow, *Latrodectus hesperus*. *Anim. Behav.* **73**, 855–864. (doi:10.1016/j.anbehav.2006.10.014)
43. Zaera R, Sanchez-Galvez V. 1998 Analytical modelling of normal and oblique ballistic impact on ceramic/metal lightweight armours. *Int. J. Impact Eng.* **21**, 133–148. (doi:10.1016/S0734-743X(97)00035-3)
44. Zaera R, Sanchez-Saez S, Perez-Castellanos J, Navarro C. 2000 Modelling of the adhesive layer in mixed ceramic/metal armours subjected to impact. *Composites A* **31**, 823–833. (doi:10.1016/S1359- 835X(00)00027-0)
45. Teran-Gilmore A, Jirsa J. 2004 The concept of cumulative ductility strength spectra and its use within performance-based seismic design. *ISET J. Earthquake Technol.* **41**, 183–200.
46. Sherman P. 1994 The orb web: an energetic and behavioral estimator of a spider's foraging and reproductive strategies. *Anim. Behav.* **48**, 19–34.(doi:10.1006/anbe.1994.1208)
47. Prestwich K. 1997 The energetics of web-building in spiders. *Comp. Biochem. Physiol. A* **57**, 321–326.(doi:10.1016/0300-9629(77)90199-2)
48. Sensenig A, Agnarsson I, Blackledge T. 2010 Behavioural and biomaterial coevolution in spider orb webs. *J. Evol. Biol.* **23**, 1839–1856. (doi:10. 1111/j.1420-9101.2010.02048.x)
49. Blackledge T, Cardullo R, Hayashi C. 2005 Polarized light microscopy, variability in spider silk diameters, and the mechanical characterization of spider silk. *Invert. Biol.* **124**, 165–173. (doi:10.1111/j.1744- 7410.2005.00016.x)
50. Liao C, Chi K, Tso I. 2009 The effects of wind on trap structural and material properties of a sit-and-wait predator. *Behav. Ecol.* **20**, 1196–1203. (doi:10. 1093/beheco/arp119)
51. Hieber C. 1984 Orb-web orientation and modification by the spiders *Araneus diadematus* and *Araneus gemmoides* (Araneae: Araneidae) in response to wind and light. *Z. Tierpsychol.* **65**, 250–260. (doi:10.1111/ j.1439-0310.1984.tb00103.x)
52. Wu C, Blamires S, Wu C, Tso I. 2013 Wind induces variations in spider web geometry and sticky spiral droplet volume. *J. Exp. Biol.* **216**, 3342–3349. (doi:10.1242/jeb.083618)
53. Heiling A, Herberstein M. 2000 Interpretations of orb-web variability: a review of past and current ideas. *Ekolo´gia* **19**, 97–106.
54. Venner S, Casas J. 2005 Spider webs designed for rare but life-saving catches. *Proc. R. Soc. B* **272**, 1587–1592. (doi:10.1098/rspb.2005.3114)
55. Blackledge T. 2011 Prey capture in orb weaving spiders: are we using the best metric? *J. Arachnol.* **39**, 205–210. (doi:10.1636/Chi10-52.1)